Available online at www.sciencedirect.com

ScienceDirect

Procedia CIRP 108 (2022) 61–65

www.elsevier.com/locate/procedia

6th CIRP Conference on Surface Integrity

Machinability of maraging steel multilayered claddings obtained via laser direct energy deposition in micromilling operations

Lucia Lizzul[a]*, Marco Sorgato[a], Rachele Bertolini[a], Andrea Ghiotti[a], Stefania Bruschi[a]

[a]*Department of Industrial Engineering, University of Padova, Via Venezia 1, 35131, Padova, Italy*

* Corresponding author. Tel.: +39 49-827 6819. *E-mail address:* lucia.lizzul@unipd.it

Abstract

Laser direct energy deposition is commonly used to improve the surface properties of poorly resistant materials, repair worn portions, or change the shape of a component. In this paper, C45 steel substrates were laser deposited with multiple layers of grade 300 maraging steel. Micromilling operations were then carried out on the laser depositions both in as-built and heat-treated conditions to improve the surface integrity. The cutting forces were measured at varying cutting directions. An in-depth characterization of the surface integrity induced by micromilling was conducted, considering microstructural features, microhardness, surface topography, and surface defects. The results proved that the laser deposition-induced anisotropy had a remarkable influence on the laser deposited material machinability and must be taken into account.

Keywords: Laser direct energy deposition; Micromilling; Surface integrity

1. Introduction

In recent years, the Laser Direct Energy Deposition (L-DED) technology has seen a significant increase in industrial applications [1]. The possibility to manufacture large parts with good metallurgical bonding, thanks to the precise control of the laser source, makes L-DED an optimal alternative to conventional manufacturing processes in several applications, most notably mold manufacturing. L-DED allows reducing production costs and material waste, as well as it can repair cracks or worn mold sections, or modify the mold design [1,2]. Regarding tool steels, maraging steels can provide an excellent alternative to typical hot working steels, such as AISI H11 and H13 [3], as they are characterized by good weldability, high ductility with high yield and tensile strengths achieved through precipitation hardening. Moreover, they have good fracture toughness and very low distortion and shrinkage as temperature changes. Despite the great potential of using L-DED maraging steels, literature records dealing with this material-technology combination still lack since most of the research on Additively Manufactured (AM) maraging steels deals with the laser powder bed fusion technology [4–6]. Because of the highly concentrated and directional heating source and high cooling rates intrinsic in the AM processes, L-DED included, the resultant microstructure differs from those of typical metallic components obtained from conventional manufacturing processes, like rolling, forging, casting. This has boosted the research on their peculiar microstructure at varying L-DED parameters as well as on its influence on post-AM operations, like machining ones. Few works took into consideration the machinability of AM maraging steels [7–9], but none dealing with L-DED ones. To give new insights in this framework, the present study deals with the machinability of L-DED grade 300 maraging steel. In particular, micromilling operations have been examined because mold inserts frequently present tiny particulars such as pins for the injected part demolding, mold cavities following the part design, cooling channels, and so on, which are typically achieved via micro-milling processes [10].

10.1016/j.procir.2022.02.194

The micromilling operations were conducted under Minimum Quantity Lubrication (MQL) conditions to explore the metal machinability at varying feed per tooth and cutting direction, the latter being parallel and perpendicular to the Laser Scanning Direction (LSD). The cutting forces, microhardness, surface topography, and surface defects were taken into consideration and correlated to the L-DED maraging steel microstructure of both the as-built and heat-treated conditions.

2. Materials and methods

2.1. Sample fabrication

Grade 300 maraging steel powders with spherical shape were utilized in this study. The particles (50-100 µm size range) were produced via vacuum inert gas atomization with nominal chemical composition reported in Table 1.

Table 1. Chemical composition of the grade 300 maraging steel powders.

Element (weight %)								
Fe	Ni	Co	Mo	Ti	Al	Si	Mn	C
Bal.	18.00	9.00	4.90	0.80	0.10	≤ 0.10	≤ 0.10	≤ 0.03

The L-DED process was performed using a diode laser with a maximum power of 3 kW and a coaxial multi-jet nozzle mounted on a robotic arm. To provide a steady flow of powder, the powder feeder utilized a rotating disk technology. The use of a shielding inert gas with a flow rate of 20 l/min reduced oxidation during the L-DED process. Grade 300 maraging steel L-DED samples with 3 layers with the same thickness were manufactured on a 15 × 15 mm^2 area of C45 steel substrate using the raster scanning strategy. The L-DED parameters were set as follows: laser power 1.3 kW, scanning speed 6.7 mm/s, track to track offset 1.1 mm, focal distance 13.8 mm, nozzle tilt angle 10°, and powder feed rate 2 rpm. This set of parameters was identified as the optimal one in a pre-testing phase as it provided homogeneous coatings with low porosity. Afterwards, a batch of L-DED samples were heat treated, using 2 different treatments, direct Annealing Treatment (AT) at 520°C for 6 hours followed by air cooling, and solution treatment at 900°C for 1 hour followed by AT at 520°C for 6 hours (SAT).

2.2. Milling trials

Non-heat-treated (NT) and heat-treated laser depositions were milled on the ultra-precision micro-milling machine Kugler™ Micromaster 5X under MQL conditions. The natural-based oil Accu-Lube™ LB 5000 was utilized as lubricant and sprayed onto the cutting zone at a rate of 150 ml/h. The cutting tools were the MS2SSD0100 end mills by Mitsubishi™. The 1 mm diameter end mill has a 2-flute sharp edge and an (Al,Ti,Cr)N coating. Before usage, each tool was inspected with a FEI™ Quanta 400 Scanning Electron Microscope (SEM) to ensure the absence of manufacturing flaws, and a new end mill was used for each cutting condition.

The machining trials consisted of full immersion slots machined parallel (//) and perpendicular (⊥) to the laser scans of the L-DED samples, which were previously flattened by grinding. Fig. 1 (a) shows the cutting directions in relation to the LSD, whereas Fig. 1 (b) and (c) report the microstructure of the transversal and longitudinal sections respectively, along the Build-up Direction (BD) of the L-DED. The cutting parameters were chosen from the tool manufacturer's datasheet. In particular, the axial depth and the tool rotation were kept constant and equal to 0.05 mm and 16000 rpm, respectively. The feed per tooth *fz* was varied, using 0.007, 0.017 and 0.025 mm/tooth. The cutting forces were recorded by using a 3-component piezoelectric dynamometer (type 9119AA2 from Kistler™) with a sampling rate of 2.5 kHz. For each sample, six measurements were carried out, and the resultant cutting force *Fres* was then calculated as the square root of the sum squares of the *Fx*, *Fy,* and *Fz* components. The experimental setup is displayed in Fig. 2.

2.3. Sample characterization after fabrication and milling

Metallographic analyses were conducted on the transversal, longitudinal and orthogonal sections in relation to the LSD. The samples were hot mounted, ground using up to 4000 grit SiC paper, and polished using a synthetic cloth with 1 µm diamond suspension. After polishing, the L-DED sections were chemically etched with 5% Nital for 60 seconds to reveal the grain boundaries. The stereo microscope Zeiss™ Stemi 2000-C was utilized for the macrostructural analyses, whilst the Leica™ DMRE optical microscope equipped with a high definition digital camera and the SEM were utilized for the microstructural characterization. The porosity of each L-DED sample was determined by image processing of ten optical micrographs obtained at 5× magnification of the three L-DED sections using the ImageJ™ software. The same software was utilized for the measurements of the other microstructural features reported in this work. In particular, twenty measurements for each feature were taken, and the mean and standard deviation were then calculated. The evaluation of the mechanical properties of the deposited layers was achieved via the Leitz™ Durimet microhardness tester with a load of 200 gf following the ASTM E92-17 standard. Thirty random indentations per each of the three L-DED sections were carried out. All the above-mentioned analyses have been carried out on the samples before their eventual heat treatment to ensure the same starting point.

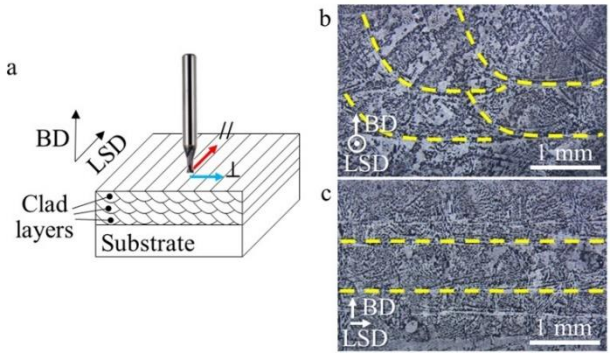

Fig. 1. Milling directions in relation to the L-DED microstructural features (a), microstructures of the transversal (b), and longitudinal (c) sections.

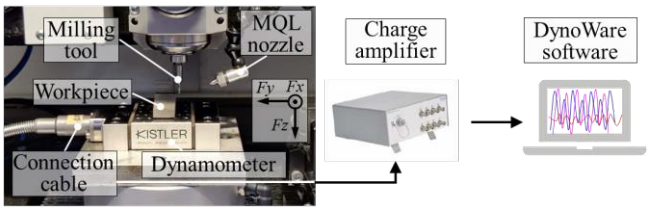

Fig. 2. Milling setup.

The surface topographies of the end-milled L-DED samples were captured using the 20× confocal objective of the Sensofar™ Plu-Neox optical profiler. For each milled slot, three 0.66 × 0.88 mm^2 scans were acquired along the slot length. The most relevant areal surface parameters to characterize a machined surface were analyzed and processed as defined in the ISO 25178 standard. In particular, the following areal parameters were considered: Sa (arithmetic mean height), Sku (kurtosis). Ssk (skewness), Spk (reduced peak height), and Svk (reduced valley depth). The machined surface defects were analyzed using the SEM backscattered electrons detector.

3. Results and discussion

3.1. Microstructure and mechanical properties

All the as-built L-DED samples presented good metallurgical bonding and an average porosity of 0.24 ± 0.12 %. As previously pointed out, the as-built L-DED samples showed an evident anisotropy because of the nature of the manufacturing process. In particular, the transversal sections showed arched fusion lines between subsequent melt pools (Fig. 1 (b)), whilst the longitudinal sections showed straight fusion lines (Fig. 1 (c)) as well as orthogonal ones. The NT samples were characterized by a mixed cellular-columnar microstructure principally composed of α martensite with traces of γ austenite (Fig. 3 (a)) [6]. After aging, the cellular-columnar microstructure is less evident (Fig. 3 (b)), even if still present, and the same applies for the melt pool boundaries. The martensite is fully transformed in austenite and the intermetallic phases precipitate along the grain boundaries [9,11]. A completely martensitic structure and further dissolution of the grain boundaries and melt pool boundaries were obtained after solution treatment because of the microstructure recrystallization. The successive aging allowed for the precipitation of the alloying elements on the former austenite grain boundaries and within the lath martensite in fine and uniform particle distribution [11], as shown in Fig. 3 (d).

The microhardness of the L-DED different sections at varying heat treatment is shown in Table 2. It was observed that the microhardness almost doubled after heat treatment, because of the precipitation of fine intermetallic compounds that greatly limit the movement of dislocations [9]. The AT samples reported, on average, the highest microhardness. The microhardness values of the SAT samples set just below (-3% on average). It is worth noting that the transversal section showed higher microhardness than the longitudinal one in the case of NT and AT samples (+7% and +15%, respectively), while the opposite was found for the SAT samples (-14%).

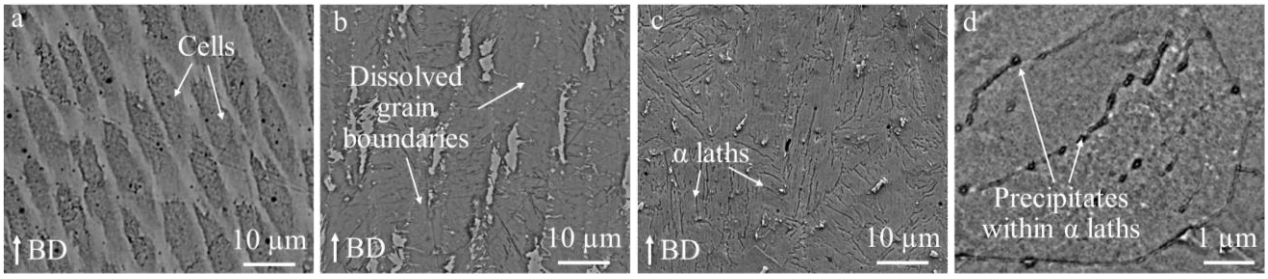

Fig. 3. Typical microstructure of the longitudinal sections of L-DED samples in NT (a), AT (b), and SAT (c) conditions. The zoomed image (d) shows the fine precipitates within the martensitic α laths in SAT condition.

The microhardness of the orthogonal sections set always in the middle. The higher microhardness in the transversal sections of the NT and AT samples can be ascribed to the higher density of the melt pool boundaries than the one in the longitudinal sections, as can be appreciated in Fig. 1. The melt pool boundaries are known to be characterized by a higher concentration of precipitates, which limits the dislocations movement [12], thus resulting in an overall increased microhardness. In the case of SAT samples, the melt pool boundaries are less evident, as above commented, and the microhardness is principally driven by the presence of precipitates in the martensitic laths. This caused the inverted trend in the microhardness values of the lateral sections. Nevertheless, more in-depth microstructural analyses will be the scope of a future work.

Table 2. Microhardness of the different sections of the L-DED samples.

$HV_{0.2}$	Transversal	Longitudinal	Orthogonal
NT	364 ± 9	340 ± 24	347 ± 20
AT	701 ± 15	608 ± 24	640 ± 22
SAT	583 ± 23	676 ± 13	635 ± 27

3.2. Cutting forces

Fig. 4 reports the resultant cutting forces when machining the L-DED samples that were differently treated at varying feed per tooth and cutting direction. It was observed that the forces increased at increasing feed per tooth as more material was proportionally removed. The cutting forces were, on average, the lowest for the NT samples and the highest for the AT ones, in accordance with the microhardness values

trend. This result points out the well-known link between the material hardness and the cutting forces [13]. In particular, the AT and SAT samples reported 36% and 21% higher cutting forces than the NT ones, respectively.

The influence of the cutting direction on the cutting forces led to different results at varying heat treatment. The cutting forces were 9% and 26% higher when cutting parallel to the LSD for NT and AT samples than when cutting perpendicular to the LSD, respectively. The opposite was verified for the SAT samples (-56% cutting forces in // direction than in ⊥ one). This is once again in accordance with the microhardness results of the different L-DED sections. As long as the melt pool boundaries are present, the mechanical properties and the machinability are governed by them (see the NT and AT cases). The solution treatment homogenizes only apparently the microstructure (the melt pool boundaries dissolve), but the microstructural anisotropy is still present and with inverted effects on machinability.

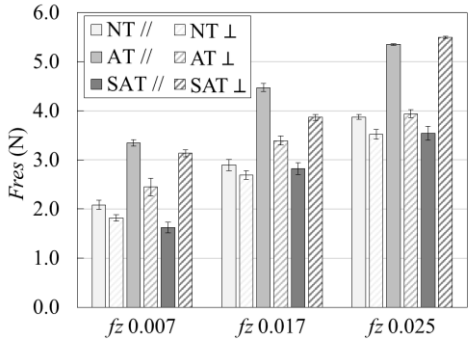

Fig. 4. Resultant cutting forces at different cutting directions and feed per tooth.

3.3. Topography of the machined surfaces

Analyzing the areal roughness parameters reported in Fig. 5, it can be observed that all the parameters increased at increasing feed per tooth, in accordance with the fact that the higher the feed marks the lower the density of peaks and the higher their height [14], thus making the final surface texture more pronounced. The increase in the roughness parameters values was found, in general, also for the heat-treated L-DED samples in relation to the non-treated ones. In particular, the AT samples reported, on average, higher roughness parameters than NT ones, and the SAT samples reported, on average, slightly higher roughness parameters than the AT ones. This is due to the fact that the harder the workpiece the higher the cutting forces, making, as a result, the finished surface more irregular [13]. It is worth noting that the average roughness *Sa* values present a similar trend to the one of the cutting forces reported in Fig. 4. The influence of the cutting direction on the roughness parameters can be distinguished, as for the cutting forces, between the NT and AT samples, which reported always the same trend, and the SAT samples that showed mostly an opposite trend.

The NT and AT samples surfaces machined parallel to the LSD reported higher *Spk*, *Svk*, and *Sa* values than those machined perpendicular to the LSD, i.e. presented higher peaks, deeper valleys, and overall higher mean roughness. The opposite was verified for the SAT samples, in accordance with the cutting force results commented in § 3.2. The only roughness parameter showing the same trend for all the L-DED samples is the skewness *Ssk*. All the surfaces machined parallel to the LSD had *Ssk* <0, whilst those machined perpendicular to the LSD had *Ssk* >0. This means that, when cutting in // direction, the resultant surfaces are mainly characterized by valleys, whilst, when cutting in ⊥ direction, the surfaces are mainly dominated by peaks. Therefore, the *Ssk* parameter can discriminate between different cutting directions when machining L-DED samples, following other findings on AM parts [15].

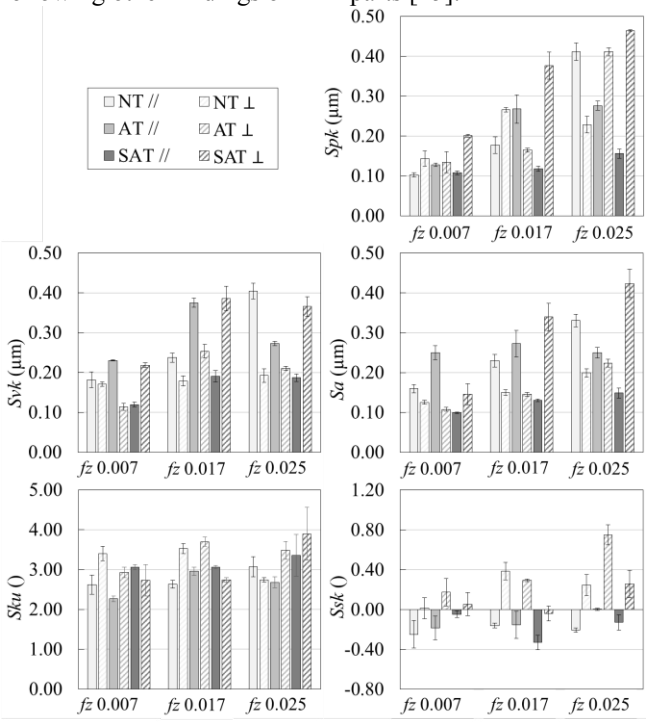

Fig. 5. Surface roughness parameters at different cutting directions and feed per tooth.

3.4. Defects of the machined surfaces

The SEM analysis of the machined surfaces showed that the feed marks were always clear, and the principal defects were smeared workpiece material at the feed marks top. Fig. 6 shows the comparison between the surfaces machined // and ⊥ to the LSD of the NT and SAT samples at fixed feed per tooth. It is possible to observe that the smeared material was present only on the surface machined parallel to the LSD in the case of the NT samples, whilst the other cutting direction led to neat and clean feed marks. The opposite was found for the SAT samples. The presence of surface defects well relates with the surface topography and cutting forces findings above commented. The higher roughness can be related to the presence of the adhered material that usually forms at those high cutting temperatures that develop when the cutting forces increase [16].

4. Conclusions

To investigate the effect of the microstructural anisotropy induced by the L-DED process on the machinability of grade

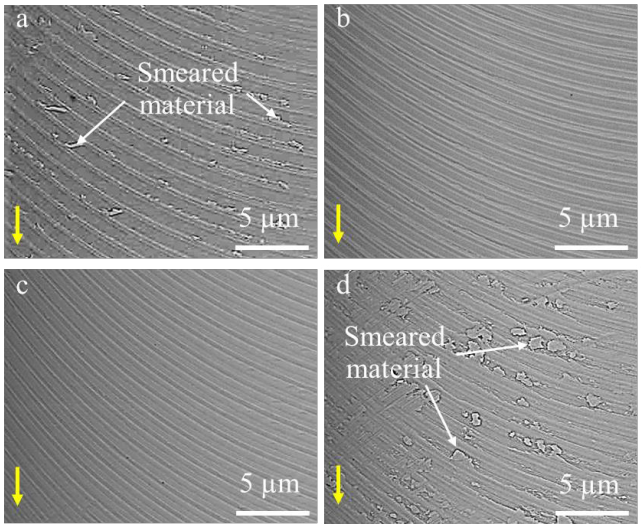

Fig. 6. SEM images of typical defects of the machined surfaces: NT sample machined // (a) and ⊥ to the LSD (b), and SAT sample machined // (c) and ⊥ to the LSD (d) (f_z 0.007 mm/tooth). The yellow arrows indicate the tool feed direction.

300 maraging steel samples, micro slotting operations in different directions were performed under MQL conditions. The machinability was evaluated in terms of cutting forces and machined surface quality, i.e. surface topography and defects, by varying the feed per tooth on three levels. In addition, different heat treatments were carried out on the L-DED samples after machining and their influence evaluated.

The main findings can be summarized as follows:

- Microstructural anisotropy dominated the L-DED samples, which showed different microstructural features, namely the melt pool boundaries were more frequent in the transversal section in relation to the laser scanning direction than in the parallel section.
- The direct aging treatment carried out on the L-DED samples dissolved part of the grain boundaries, but do not dissolve the melt pool boundaries. On the contrary, the solution treatment was able to partially dissolve the melt pool boundaries and homogenize the L-DED sample microstructure.
- The presence of the melt pool boundaries controlled the microhardness of the different sections: in the case of non-treated and aged L-DED samples, the transversal sections were harder because of the presence of precipitates at the melt pool boundaries. The opposite was found for solution treated and aged L-DED samples.
- The cutting forces were higher when cutting parallel to the laser scanning direction than perpendicular to it in the non-treated and aged samples. The opposite was found for solution treated and aged L-DED samples, in accordance to the microhardness values.
- The surface mean roughness *Sa* had the same trend of the cutting forces. The skewness *Ssk* roughness parameter well discriminated between surfaces machined parallel ($Ssk < 0$) and perpendicular ($Ssk > 0$) to the laser scanning direction.
- The higher roughness parameters values of the machined surfaces corresponded to the presence of smeared material on the surfaces themselves.

Acknowledgments

The Authors would like to express their gratitude to Standex Engraving Mold-Tech S.r.l. for supplying the L-DED samples.

References

[1] Zhu L, Xue P, Lan Q, Meng G, Ren Y, Yang Z, et al. Recent research and development status of laser cladding: A review. Opt Laser Technol 2021;138.

[2] Cabeza M, Castro G, Merino P, Pena G, Román M. Laser surface melting: A suitable technique to repair damaged surfaces made in 14 Ni (200 grade) maraging steel. Surf Coatings Technol 2012;212:159–68.

[3] Grum J, Slabe JM. Possibility of introducing laser surfacing into maintenance service of die-casting dies. Surf Coatings Technol 2004;180–181:596–602.

[4] Mutua J, Nakata S, Onda T, Chen ZC. Optimization of selective laser melting parameters and influence of post heat treatment on microstructure and mechanical properties of maraging steel. Mater Des 2018;139:486–97.

[5] Casalino G, Campanelli SL, Contuzzi N, Ludovico AD. Experimental investigation and statistical optimisation of the selective laser melting process of a maraging steel. Opt Laser Technol 2015;65:151–8.

[6] Bodziak S, Al-rubaie KS, Dalla L, Humel F, Costa E, Marcon A, et al. Materials Characterization Precipitation in 300 grade maraging steel built by selective laser melting: Aging at 510 ° C for 2 h 2019;151:73–83.

[7] Du W, Bai Q, Zhang B. Machining characteristics of 18Ni-300 steel in additive / subtractive hybrid manufacturing. Int J Adv Manuf Technol 2018;95:2509–19.

[8] Fortunato A, Lulaj A, Melkote S, Liverani E, Ascari A, Umbrello D. Milling of maraging steel components produced by selective laser melting. Int J Adv Manuf Technol 2018;94:1895–902.

[9] Bai Y, Zhao C, Yang J, Hong R, Weng C, Wang H. Microstructure and machinability of selective laser melted high-strength maraging steel with heat treatment. J Mater Process Technol 2021;288:116906.

[10] Parenti P, Masato D, Sorgato M, Lucchetta G, Annoni M. Surface footprint in molds micromilling and effect on part demoldability in micro injection molding. J Manuf Process 2017;29:160–74.

[11] Tan C, Zhou K, Ma W, Zhang P, Liu M, Kuang T. Microstructural evolution, nanoprecipitation behavior and mechanical properties of selective laser melted high-performance grade 300 maraging steel. Mater Des 2017;134:23–34.

[12] Hovig EW, Azar AS, Solberg K, Sorby K. An investigation of the anisotropic properties of heat-treated maraging steel grade 300 processed by laser powder bed fusion. Int J Adv Manuf Technol 2021;114:1359–72.

[13] Özel T, Hsu TK, Zeren E. Effects of cutting edge geometry, workpiece hardness, feed rate and cutting speed on surface roughness and forces in finish turning of hardened AISI H13 steel. Int J Adv Manuf Technol 2005;25:262–9.

[14] Grzesik W. Advanced Machining Processes of Metallic Materials: Theory, Modelling, and Applications. second. Elsevier; 2017.

[15] Lizzul L, Sorgato M, Bertolini R, Ghiotti A, Bruschi S. Anisotropy effect of additively manufactured Ti6Al4V titanium alloy on surface quality after milling. Precis Eng 2021;67.

[16] Zhang PR, Liu ZQ, Guo YB. Machinability for dry turning of laser cladded parts with conventional vs. wiper insert. J Manuf Process 2017;28:494–9.